Applied Surface Science 282 (2013) 538–543

Contents lists available at SciVerse ScienceDirect

Applied Surface Science

journal homepage: www.elsevier.com/locate/apsusc

Visible light photoelectrochemical properties of β-Bi_2O_3 nanoporous films: A study of the dependence on thermal treatment and film thickness

Xin Yang[a,b], Xiaojuan Lian[a,b], Shangjun Liu[a], Chunping Jiang[a], Jing Tian[a], Gang Wang[a], Jinwei Chen[a], Ruilin Wang[a,*]

[a] College of Materials Science and Engineering, Sichuan University, Chengdu, China
[b] Chongqing Key Laboratory of Micro/Nano Materials Engineering and Technology, Chongqing University of Arts and Sciences, 402160 Chongqing, China

ARTICLE INFO

Article history:
Received 7 February 2013
Received in revised form 14 May 2013
Accepted 2 June 2013
Available online 11 June 2013

Keywords:
β-Bi_2O_3 films
Nanoporous
AFM
Photoelectrochemical
IPCE

ABSTRACT

Bi_2O_3 thin films were successfully prepared on fluorine doped SnO_2 substrate by the sol–gel route. The effects of annealing temperature on the film structure and photoelectrochemical (PEC) performance were also discussed. Bi_2O_3 thin films were characterized by conventional techniques. X-ray diffraction (XRD) results show the 450 °C annealed film exhibits β-phase structure with the best crystallinity. Scanning electron microscope (SEM) analysis indicates that the surface morphology varies with changing the annealing temperature. The film surface becomes nanoporous at high annealing temperature. Atomic force microscope (AFM) result indicates that the grains on the surface still exhibit close-packed growth in the nanoscale, even though there are many holes in the film surface. The photoelectrochemical performance was evaluated by incident photon-to-current conversion efficiency (IPCE). The IPCE reaches 10.5% at 400 nm (25.5% at 350 nm) without any additional potential vs. Ag/AgCl in 1 M NaOH solution.

1. Introduction

In the last decades, production of hydrogen by solar energy motivated scientists in the investigation of new, safe, clean and low cost technologies. A large number of researches have been focused on semiconductor photocatalyst used for water splitting [1–3] and water purification [4,5] under ultra violet and visible light irradiation. Hitherto TiO_2 was the most commonly used photocatalyst with well UV region photoelectrochemical (PEC) performance. However, the band gap of TiO_2 is too wide to utilize visible light, which corresponds to 46% of the solar spectrum. Bismuth based oxides, with a relatively narrow band gap, appear to be promising candidates for the visible light photocatalyst. Bi_2O_3 is an direct transition band semiconductor with E_g = 2.8 eV [6]. It has been synthesized by solid-state reaction [7,8], sono-chemical method [9], electro deposition [10,11], and hydrothermal route [12–15]. Many Bi_2O_3 photocatalysts with good photo activity have been reported so far. The sono-chemical synthesized monoclinic nanocrystallite Bi_2O_3 could degrade 86% of the methyl orange in 100 min under visible light illumination [9]. The photocatalytic of nanocrystallite Bi_2O_3 was greatly superior to that of micro-size Bi_2O_3 and TiO_2 (P25). Cubic mesoporous films and nanofibers mats were synthesized with two different methods and both materials were highly crystalline after thermal treatment and the benefits of a mesoporous morphology in heterogeneous semiconductor photocatalysis were confirmed [16]. The low pressure chemical vapor deposition (LPCVD) fabricated β-Bi_2O_3 showed well oxygen oxidation ability from water when illuminated and the calculated quantum yield efficiency was about 9.8% at 365 nm [17]. However, the visible light photo activity was still unsatisfied. β-Bi_2O_3 nanofibers were prepared by electro-spinning a precursor mixture of polyacrylonitrile/bismuth-nitrate, and then annealed at different temperatures. The photo activity was high for photo degradation of Rhodamine B and the photo activity did not decrease after illumination [18]. Recently, nanoporous β-Bi_2O_3 thin film showed enhanced photoelectrochemical performance, because the nanoporous morphology could enlarge the film surface/electrolyte contact area than the plane surface and morphology, which ultimately contributed to the charge separation [19], and the IPCE reached 43% at 400 nm (0.197 V vs. NHE).

During the last decade, not only pure β-Bi_2O_3, but also doping with different elements or combining with other photoactive materials [20–23] were investigated in order to improve the photocatalysis performance. The Ti-doped β-Bi_2O_3 was chemical stable yet after degrading three kinds of dyes [10,24]. The 2.0 wt% Ag doped β-Bi_2O_3 showed the best photo activity by degradation of

* Corresponding author.
E-mail address: rl.wang@scu.edu.cn (R. Wang).

0169-4332/$ – see front matter © 2013 Elsevier B.V. All rights reserved.
http://dx.doi.org/10.1016/j.apsusc.2013.06.007

Rhodamine B among different content doping. Ag in β-Bi_2O_3 lattice was good for the migration of the photo-generated carriers, leading to a higher visible light photo catalytic performance [25].

Sol–gel spin coating is a low cost and easy operating film-preparation method [26]. However, until now no detailed report on the PEC property of β-Bi_2O_3 film fabricated by sol–gel spin coating appeared in the literature to our knowledge. Herein we report on the fabrication, photoelectrochemical characterization and photoactivity of β-Bi_2O_3 thin film with different thermal treatment. The PEC properties are evaluated by incident photon to current conversion efficiency (IPCE) and absorbed photon to conversion efficiency (APCE). The optimum thickness with the highest conversion efficiency of β-Bi_2O_3 film is also determined.

2. Experiment

2.1. Materials preparation and characterization

All the chemical reagents were used as purchased without further purification. First, 0.8 mL of nitric acid was added slowly into 4 mL deionized water. Then 1 g of $Bi(NO_3)_3{\cdot}5H_2O$ was added into the solution. The solution was marked as solution A. The two steps were all under continuous stirring. 0.8 mL of triton X-100 and certain content citrate acid were dissolved in 2 mL of ethanol. This solution was marked with solution B. Solution B was drop wise added into solution A and then stirred for 4 h to form stable solution mixture. After that, the mixture was aged for 12 h. The fluorine-doped tin oxide glass (FTO) was ultrasonic cleaned in sequence of soap water, acetone and ethanol sequentially. The film was prepared with (KW-4A) spin coating instrument. In order to find out the thermal treatment dependence, each film was annealed in air at different temperature (heating rate 3 °C/min) for 2 h in a tube furnace after pre-heat treatment (100 °C for 30 min), and then cooled to room temperature. The optimum thickness was obtained at the best heat treatment temperature.

The film thickness was measured by KLA Tencor D-100 step-profiler. XRD was used to characterize the phase state in a scanning range of 20–70° (2θ) (Cu Kα_1 radiation, λ = 1.54056 Å, 40 kV, 25 mA). UV–visible absorbance spectra were measured to study the light harvesting ability. Clean blank FTO glass was used as the standard baseline. The surface morphology was characterized by S-4800 scanning electron microscope and CSPM-4000 model atomic force microscope.

2.2. Photoelectrochemical performance test

The IPCE measurements were carried out in a three-arm vessel fitted by quartz window in 1.0 M NaOH solution. The system was composed of an SBP500 monochromator, a potential stat, a Lock-in Amplifier, one calibrated silicon dioxide, and one 150 W Xeon Lamp. Polyimide sealed β-Bi_2O_3 film was used as working electrode, a graphite rod was used as the counter electrode, and Ag/AgCl (saturated KCl solution) as the reference electrode.

3. Results and discussion

3.1. X-ray diffraction

All prepared samples exhibit well-crystallized phase (Fig. 1). The films display a tetragonal structure according to JCPDS 27-0050 (β-Bi_2O_3, $a = b = 7.741$ Å, $c = 5.634$ Å). Among the five different thermal treatment temperature, the 450 °C sample shows the strongest (2 0 1) and (2 2 0) diffraction peaks. Unlike the electro-spun fabricated nanofibers [18], there is no clear α-phase characteristic peaks appearing when the annealing temperature rises to 550 °C. The

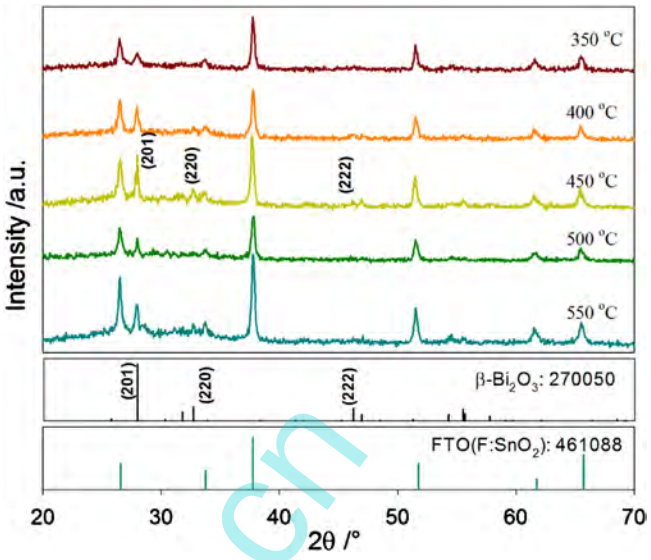

Fig. 1. XRD patterns of Bi_2O_3 thin films after thermal treated at five different temperatures.

phase change may be slight and the instrument precision is not enough. Compared with other β-Bi_2O_3 prepared with prolonged annealing time under O_2 condition [27], all films in this experiment exhibit major phase of tetragonal β-Bi_2O_3. As a result, the thermal treatment temperature and O_2 condition are the key elements causing the phase transition of β-Bi_2O_3 → α-Bi_2O_3. Short annealing time or non-full O_2 condition may not induce Bi_2O_3 phase transition. Samples annealed at lower temperature (350 and 400 °C) show weaker peak intensity than the 450 °C one. Another two samples treated at higher temperature (500 and 550 °C) also exhibit weaker peak intensity. The mean crystallite size are calculated from Debye–Scherrer's formula: $D = K\lambda/(\beta\cos\theta)$. Here D is the crystallite mean dimension, K is the Scherrer constant ($K = 0.94$), λ is the wavelength of Cu Kα_1, β is the full width at half maximum and θ is the Bragg diffraction angle. The calculation is based on the (2 0 1) peak. As shown in Fig. 4, the estimated crystallite size of each film with annealing temperature increasing is about 20 nm, 29 nm, 40 nm, 34 nm and 32 nm, respectively. The reason for the small crystallite size of low temperature samples is that there is not enough thermodynamic energy for the grain growing at low temperature annealing and organic residue is not fully removed. At 500 and 550 °C, some slight phase change might have occurred during the annealing process, which causes the mean crystallite size becoming small.

3.2. Optical absorption and band gap

Optical absorption curves are shown in Fig. 2a. There are two obvious absorption edges for the prepared films. The first one is located around 460 nm and the second one is located at about 380 nm, which corresponds to the photon energy 2.70 eV and 3.26 eV, respectively. Based on the band structure calculation, the valence band maximum of Bi_2O_3 is attributed to O 2p, Bi 6s and Bi 6p hybridization, while the conduction band minimum is composed of the hybridization of O 2p and Bi 6p. Therefore, the two absorption edges may come from the photon-electron excitation in the form of O 2p → Bi 6p and Bi 6s → Bi 6p [9,14]. For a direct band gap semiconductor, the optical band gap is expressed by the formula: $(\alpha h\upsilon)^2 \propto A\left(h\upsilon - E_g\right)$, where α, h, ν, E_g and A correspond to absorption coefficient, Planck constant, light frequency, band gap and proportionality constant, respectively. Fig. 2b shows the plots of direct transition fitting of all films. With annealing

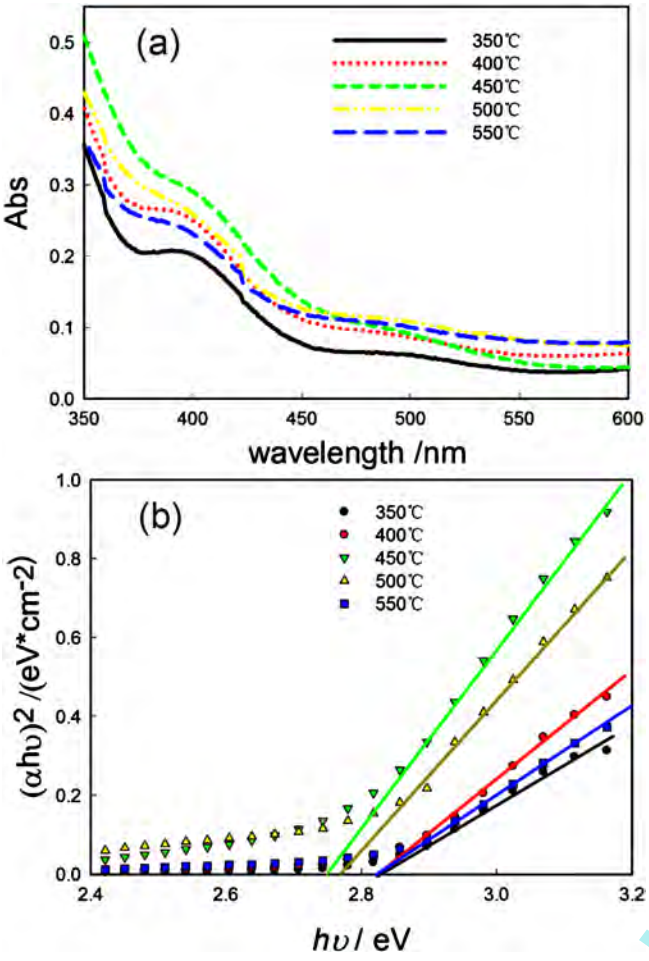

Fig. 2. UV–visible light absorbance spectra (a) and direct transition fitting vs. photon energy of β-Bi_2O_3 thin films.

temperature increasing from 350 °C to 450 °C, E_g becomes narrower and reaches about 2.74 eV, which means more visible light can be absorbed under the same irradiation. The band gap becomes wider with the temperature rising from 450 °C to 550 °C.

3.3. SEM morphology

The low magnification SEM images show a clear distinction among the five samples (Fig. 3). The particle size of each film is different with changing thermal treatment temperature. Both the low temperature (Fig. 3a and b) annealed films exhibit dense arranged surface with small particles, which can be assumed as plane surface. As the annealing temperature rises to 450 °C, the particle grows larger and there is much empty room among particles. The particle size is also in good uniformity on the surface (50–100 nm). When films were treated under higher temperature, surface particles become larger. However, the particle size distribution is much more non-uniform (Fig. 3d and e). The 450 °C treated film possesses the biggest crystallite and the smallest particle size distribution at the same time (Fig. 4), so the grain aggregation is smaller than other samples. As a result, its electro property may have superiority over other four samples. Fig. 3f shows that the detail information of the 450 °C sample, there are many holes in the surface, which enable the electrolyte to permeate into the film surface, reacting directly with the photo generated holes [19,28,29].

3.4. AFM analysis

Fig. 5 shows the surface structure, three-dimension surface and section analysis of the red rectangle marked area of the 450 °C treated film. The surface morphology analysis conforms to SEM results in the 500 nm × 500 nm scale. The grains on the surface still exhibit close-packed growth in the nanoscale, even though there are many holes around them. In addition, the particle size is well distributed and in accordance with SEM analysis. The surface undulation of this micro area is about 136 nm, which contributes to the charge transfer process in the water oxidation process.

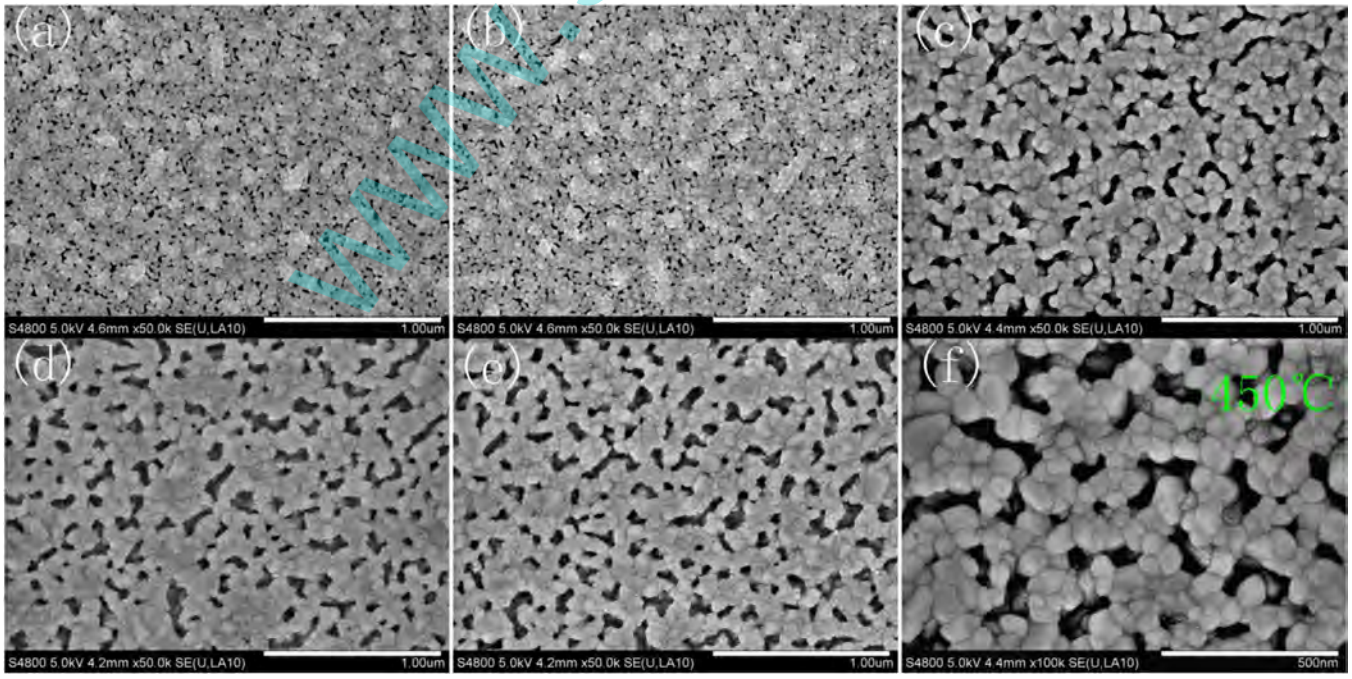

Fig. 3. SEM images of thin films: 350 °C (a), 400 °C (b), 450 °C (c), 500 °C (d), 550 °C (e) and high magnification image of 450 °C sample.

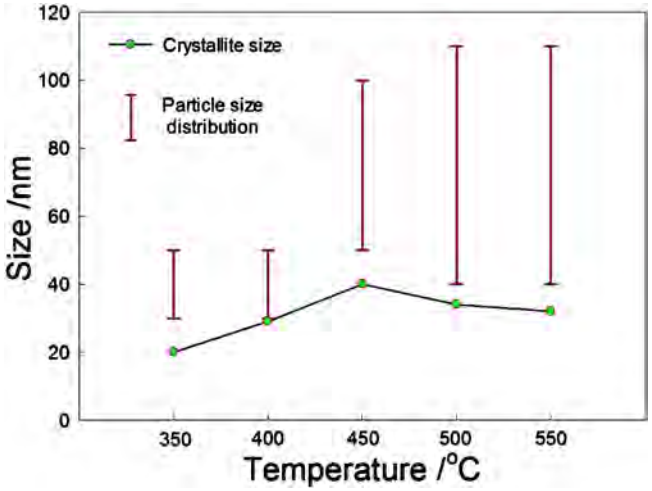

Fig. 4. Mean crystallite size estimated from XRD patterns and particle size distribution of films treated under different temperature.

3.5. IPCE and APCE

The photoelectrochemical performance was evaluated by the incident photon-to-current conversion efficiency (IPCE) and absorbed photon-to-electron current conversion efficiency (APCE). The IPCE is defined as:

$$\mathrm{IPCE}\,(\%) = \frac{I}{P}\frac{1240}{\lambda} \times 100$$

here, I is the photocurrent density (mA cm^{-2}). P is the power of monochromatic light irradiated on the electrode (mW cm^{-2}) and λ is the incident light wavelength (nm). The measurement is performed under 0 V bias vs. Ag/AgCl. Fig. 6a shows that as the annealing temperature rising to 450 °C, the IPCE increases from 3.1% to 26% at 350 nm irradiation. As the temperature increases to 550 °C, IPCE decreases from 26% to 16% at 350 nm. At the visible light region ($\lambda \geq 400$ nm), the higher temperature treated films show higher IPCE than that of the lower temperature treated ones, and the best annealing temperature is about 450 °C. Compared with the nanoporous β-Bi_2O_3 thin film prepared by magnetron sputtering (43% at 400 nm) [19], the sol–gel spin coated films exhibit less photocatalytic property, because during the annealing process, the organic substance will not fully decompose, especially under low temperature process. However, the 450 °C treated sample still possesses three advantages in comparison with other four films: (1) It obtains the uniform crystallite with a mean crystallite size about 40 nm, and there is few aggregation on the films surface (Fig. 5). As a result, the grain boundaries are much few than other films and photogenerated carriers in the depletion layer could transfer from the surface to the back contact electrode more easily rather than recombining with each other rapidly. Thus, the bulk recombination could be reduced. Although the 500 and 550 °C have nearly the same particle size, the mean crystallite size of those films is smaller, and the particle size distribution is bigger than the 450 °C film. Therefore, there are more grain boundaries in the bulk film, which finally block the electron transferring and reduce the photoelectrochemical property. As about the 350 and 400 °C films, there are hardly any big grains formed during the annealing process, the electron

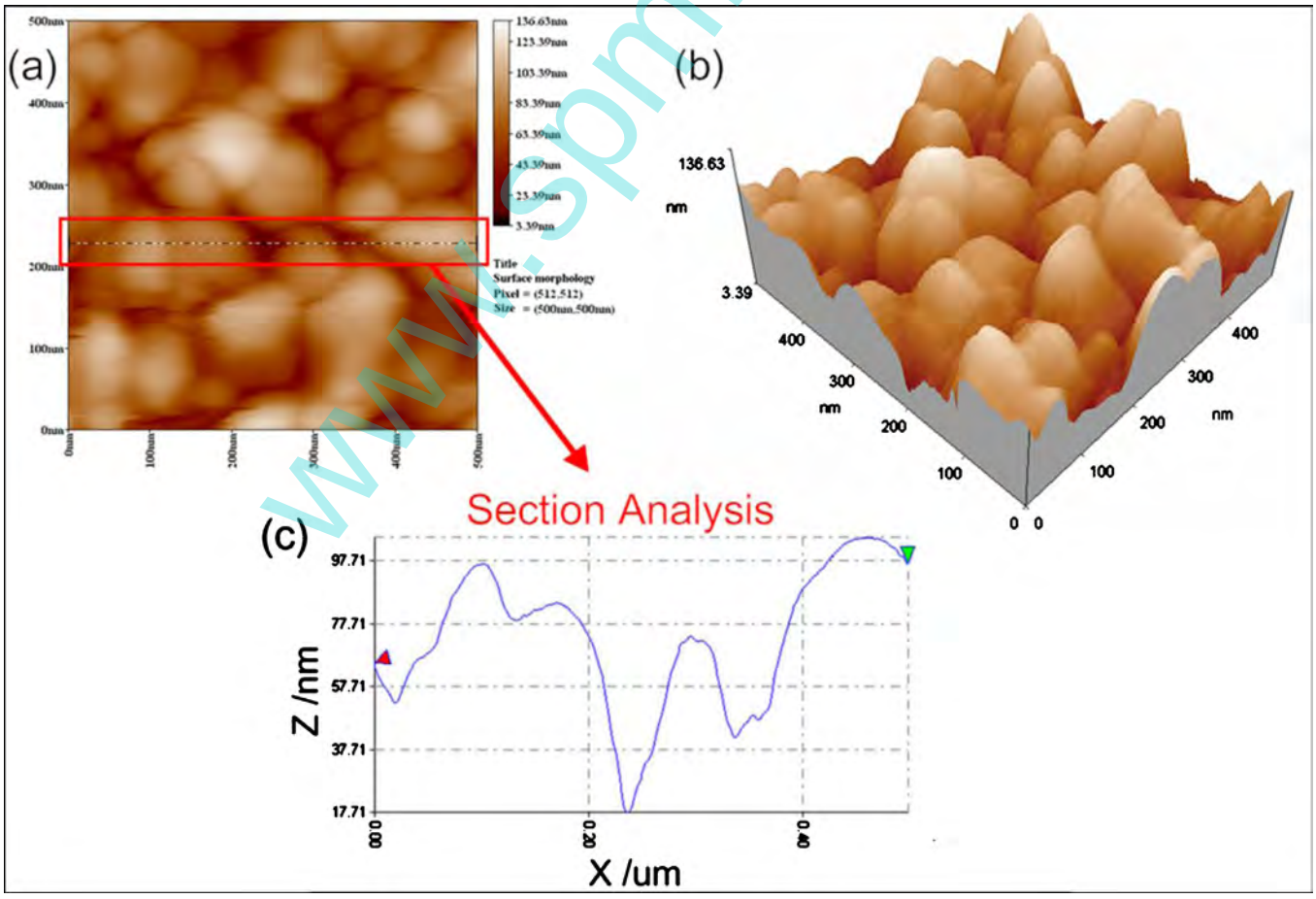

Fig. 5. AFM surface structure (a), three dimension image (b) and section analysis (c) of the 450 °C treated film.

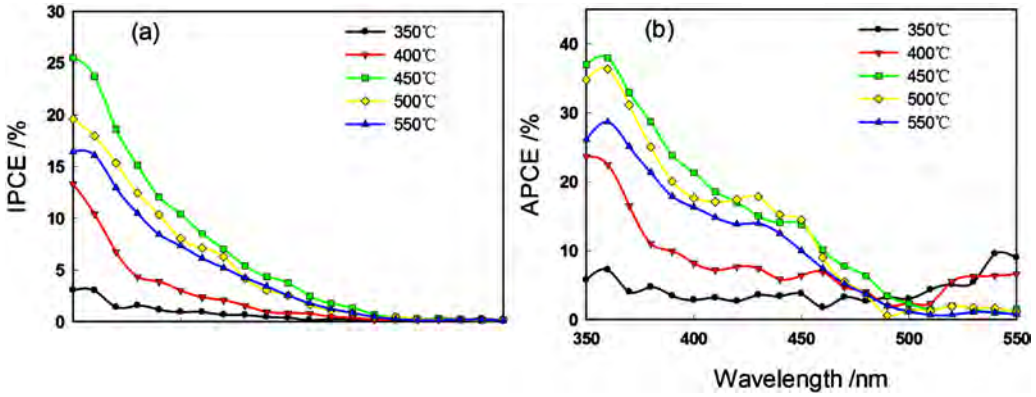

Fig. 6. IPCE (a) and APCE (b) of each film heat-treated under different temperature with bias of 0 V vs. Ag/AgCl in 1 M NaOH, pH ≈ 13.6.

transferring process is obstructed. (2) The nanoporous surface morphology benefits the charge separation process on the film surface. The electrolyte can permeate the holes on the surface and enlarge the contact area between particles and electrolyte, resulting in the directly reaction between photogenerated holes and electrolyte. (3) The energy gap of the 450 °C treated film possesses the narrowest band gap among all films. More light can be absorbed with narrower the band gap. It could produce more photo-generated carriers at the same time compared with wider band gap films.

The APCE is another parameter to evaluate the photo anode and defined by the formula below [30]:

$$\mathrm{APCE} = \frac{\mathrm{IPCE}}{1 - 10^{-A}}$$

here A is the absorbance. $(1–10^{-A})$ represents the light harvesting efficiency (LHE) of the film. The highest APCE is obtained from the 450 °C treated film (37% at 350 nm, 0 V vs. Ag/AgCl, Fig. 6b).

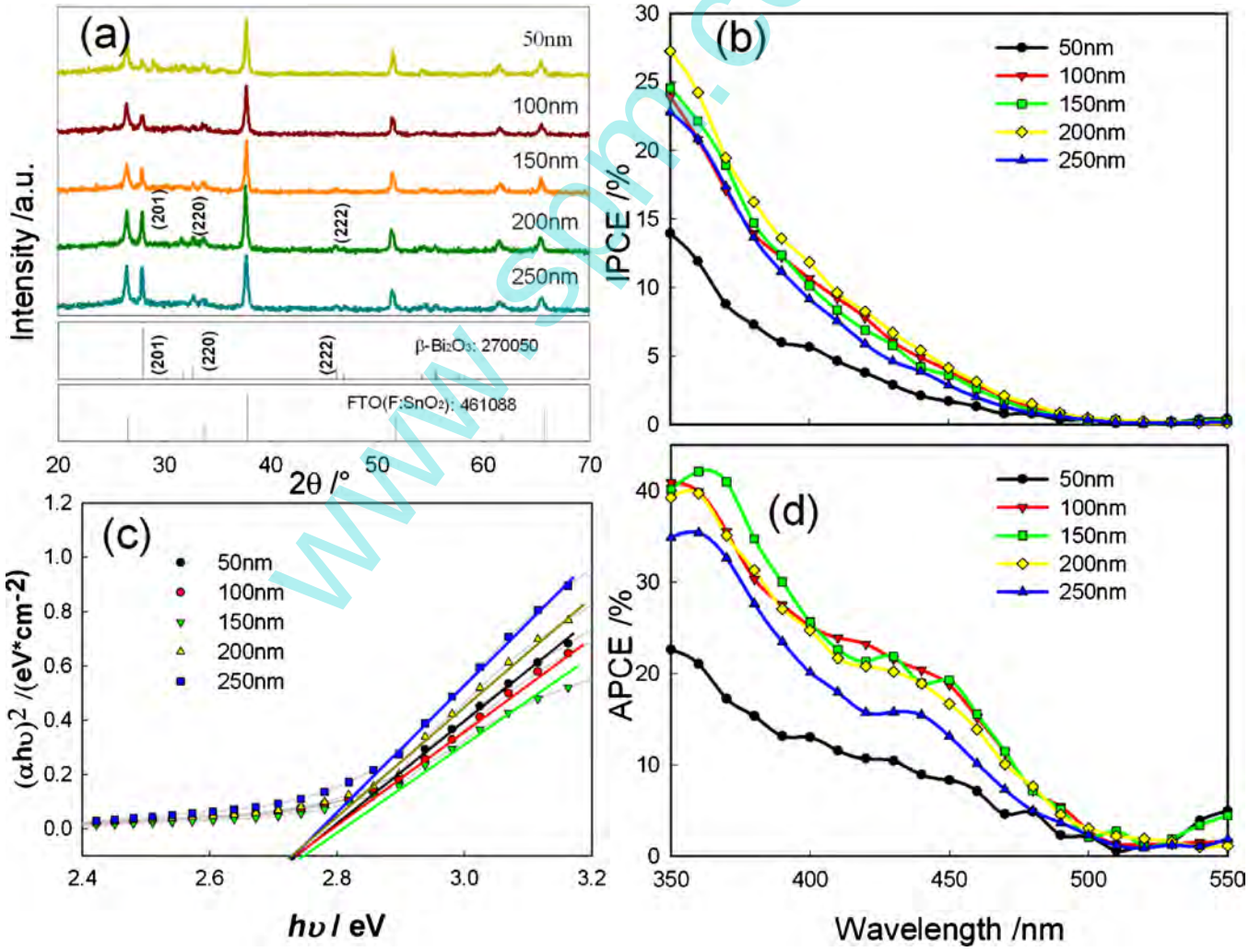

Fig. 7. XRD patterns (a), IPCE (b), band gap fitting (c), and APCE (d) of each film heat-treated under different temperature with 0 V vs. Ag/AgCl in 1 M NaOH, pH ≈ 13.6.

The APCE variation tendency is the same like IPCE curves, which means the 450 °C treated film not only absorbs maximum light among five films, but also can transform the photons to current most effectively.

3.6. Optimum thickness of β-Bi_2O_3 film

The film dependence of the photoelectrochemical property was also determined. Five different thickness films were prepared under 450 °C annealing. Fig. 7a shows the major peak intensity increases with the film thickness becoming thick. The band gaps of five films are almost the same derived from the α^2–$h\upsilon$ relation (Fig. 7c). The band gap is located at 2.72 eV. The 200 nm film obtained the highest IPCE among five films, while its APCE is lower than the 150 nm film. However, IPCE could enunciate the real performance of the film anode. Therefore, the optimum thickness of β-Bi_2O_3 is about 200 nm.

4. Conclusions

β-Bi_2O_3 thin films with different photoelectrochemical properties have been successfully prepared by sol–gel spin coating method. The nanoporous surface structure is formed during thermal treatment under different temperature. The 450 °C treated film has the best crystallinity and the biggest mean crystallite size. There is little aggregation on the film surface and surface particles bind with each other tightly from the SEM and AFM morphology analysis. IPCE and APCE results show that the photoelectrochemical performance is strongly depending on the thermal treatment temperature. The 450 °C treated film obtained both highest IPCE and APCE, which is 26% and 37% at 350 nm (0 V vs. Ag/AgCl), respectively. Three conditions advance the photoelectrochemical property of the 450 °C treated film from the analysis. Tuning the thickness can get different photoactive films; the best film thickness is about 200 nm.

Acknowledgements

This research is supported by 863 project (2006AA05Z102), collaborative innovation fund by China Academy of Engineering Physics and Sichuan University (No XTCX2011001), Sichuan Provincial Department of Science and Technology R&D Program (2013FZ0034), and Specialized Research Fund for the Doctoral Program of Higher Education (20110181110003). Specially thank Prof. Zhu Shifu for the XRD and SEM analysis.

References

[1] H.M. Chen, C.K. Chen, R.-S. Liu, L. Zhang, J. Zhang, D.P. Wilkinson, Nano-architecture and material designs for water splitting photoelectrodes, Chemical Society Reviews 41 (2012) 5654–5671.
[2] T. Majima, T. Tachikawa, Single-molecule, single-particle fluorescence imaging of TiO_2-based photocatalytic reactions, Chemical Society Reviews 39 (2010) 4802–4819.
[3] X.B. Chen, S.H. Shen, L.J. Guo, S.S. Mao, Semiconductor-based photocatalytic hydrogen generation, Chemical Reviews 110 (2010) 6503–6570.
[4] P. Baldrian, V. Merhautova, J. Gabriel, F. Nerud, P. Stopka, M. Hruby, M.J. Benes, Decolorization of synthetic dyes by hydrogen peroxide with heterogeneous catalysis by mixed iron oxides, Applied Catalysis B: Environmental 66 (2006) 258–264.
[5] C.A. Grimes, O.K. Varghese, S. Ranjan, Oxide semiconducting materials as photoanodes, in: Light, Water, Hydrogen, 2008, pp. 191–255.
[6] P. Maruthamuthu, K. Gurunathan, E. Subramanian, M.V.C. Sastri, Visible light-induced hydrogen production from water with $Pt/Bi_2O_3/RuO_2$ in presence of electron relay and photosensitizer, International Journal of Hydrogen Energy 19 (1994) 889–893.
[7] J. Eberl, H. Kisch, Visible light photo-oxidations in the presence of α-Bi_2O_3, Photochemical & Photobiological Sciences 7 (2008) 1400–1406.
[8] A.P. Finlayson, E. Ward, V.N. Tsaneva, B.A. Glowacki, Bi_2O_3-WO_3 compounds for photocatalytic applications by solid state and viscous processing, Journal of Power Sources 145 (2005) 667–674.
[9] L. Zhang, W. Wang, J. Yang, Z. Chen, W. Zhang, L. Zhou, S. Liu, Sonochemical synthesis of nanocrystallite Bi_2O_3 as a visible-light-driven photocatalyst, Applied Catalysis A: General 308 (2006) 105–110.
[10] L. Yin, J. Niu, Z. Shen, Y. Sun, The electron structure and photocatalytic activity of Ti(IV) doped Bi_2O_3, Science China Chemistry 54 (2011) 180–185.
[11] N. Myung, S. Ham, S. Choi, Y. Chae, W.G. Kim, Y.J. Jeon, K.J. Paeng, W. Chanmanee, N.R. de Tacconi, K. Rajeshwar, Tailoring interfaces for electrochemical synthesis of semiconductor films: $BiVO_4$, Bi_2O_3, or composites, Journal of Physical Chemistry C 115 (2011) 7793–7800.
[12] Q. Yang, Y. Li, Q. Yin, P. Wang, Y.-B. Cheng, Hydrothermal synthesis of bismuth oxide needles, Materials Letters 55 (2002) 46–49.
[13] Z.W. Chen, J.Q. Hu, X.H. He, Controllable growth of monoclinic alpha-Bi_2O_3 submicrorods by hydrothermal synthesis method, Rare Metal Materials and Engineering 39 (2010) 26–30.
[14] M. Ge, Y. Li, L. Liu, Z. Zhou, W. Chen, Bi_2O_3–Bi_2WO_6 composite microspheres: hydrothermal synthesis and photocatalytic performances, Journal of Physical Chemistry C 115 (2011) 5220–5225.
[15] J.K. Reddy, B. Srinivas, V.D. Kumari, M. Subrahmanyam, Sm^{3+}-doped Bi_2O_3 photocatalyst prepared by hydrothermal synthesis, Chemcatchem 1 (2009) 492–496.
[16] K. Brezesinski, R. Ostermann, P. Hartmann, J. Perlich, T. Brezesinski, Exceptional photocatalytic activity of ordered mesoporous β-Bi_2O_3 thin films and electrospun nanofiber mats, Chemistry of Materials 22 (2010) 3079–3085.
[17] S.J.A. Moniz, C.S. Blackman, C.J. Carmalt, G. Hyett, MOCVD of crystalline Bi_2O_3 thin films using a single-source bismuth alkoxide precursor and their use in photodegradation of water, Journal of Materials Chemistry 20 (2010) 7881–7886.
[18] C.H. Wang, C.L. Shao, L.J. Wang, L. Zhang, X.H. Li, Y.C. Liu, Electrospinning preparation, characterization and photocatalytic properties of Bi_2O_3 nanofibers, Journal of Colloid and Interface Science 333 (2009) 242–248.
[19] X. Yang, X. Lian, S. Liu, G. Wang, C. Jiang, J. Tian, J. Chen, R. Wang, Enhanced photocatalytic performance: a β-Bi_2O_3 thin film by nanoporous surface, Journal of Physics D: Applied Physics 46 (2013) 035103.
[20] B. Naik, K.M. Parida, G.C. Behera, Facile synthesis of $Bi_2O_3/TiO_{2-x}N_x$ and its direct solar-light-driven photocatalytic selective hydroxylation of phenol, Chemcatchem 3 (2011) 311–318.
[21] T. Saison, N. Chemin, C. Chaneïac, O. Durupthy, V.r. Ruaux, L. Mariey, F.o. Maugeï, P. Beaunier, J.-P. Jolivet, Bi_2O_3, $BiVO_4$ and Bi_2WO_6: impact of surface properties on photocatalytic activity under visible light, Journal of Physical Chemistry C 115 (2011) 5657–5666.
[22] N.T. Hahn, S. Hoang, J.L. Self, C.B. Mullins, Spray pyrolysis deposition and photoelectrochemical properties of n-type BiOI nanoplatelet thin films, ACS Nano 6 (2012) 7712–7722.
[23] R. Saito, Y. Miseki, K. Sayama, Highly efficient photoelectrochemical water splitting using a thin film photoanode of $BiVO_4/SnO_2/WO_3$ multi-composite in a carbonate electrolyte, Chemical Communications 48 (2012) 3833–3835.
[24] Y. Wang, Y.Y. Wen, H.M. Ding, Y.K. Shan, Improved structural stability of titanium-doped beta-Bi_2O_3 during visible-light-activated photocatalytic processes, Journal of Materials Science 45 (2010) 1385–1392.
[25] G.Q. Zhu, W.X. Que, J. Zhang, Synthesis and photocatalytic performance of Ag-loaded beta-Bi_2O_3 microspheres under visible light irradiation, Journal of Alloys and Compounds 509 (2011) 9479–9486.
[26] L. Xiaojuan, Y. Xin, L. Shangjun, X. Ying, J. Chunping, C. Jinwei, W. Ruilin, Enhanced photoelectrochemical performance of Ti-doped hematite thin films prepared by the sol-gel method, Applied Surface Science 258 (2012) 2307–2311.
[27] M. Gotić, S. Popović, S. Musić, Influence of synthesis procedure on the morphology of bismuth oxide particles, Materials Letters 61 (2007) 709–714.
[28] M.A. Perez, M.L. Teijelo, Cathodic behavior of bismuth. I. Ellipsometric study of the electroreduction of thin Bi_2O_3 films, Journal of Electroanalytical Chemistry 583 (2005) 212–220.
[29] V.M. Aroutiounian, V.M. Arakelyan, G.E. Shahnazaryan, Metal oxide photoelectrodes for hydrogen generation using solar radiation-driven water splitting, Solar Energy 78 (2005) 581–592.
[30] K. Sivula, R. Zboril, F. Le Formal, R. Robert, A. Weidenkaff, J. Tucek, J. Frydrych, M. Gratzel, Photoelectrochemical water splitting with mesoporous hematite prepared by a solution-based colloidal approach, Journal of the American Chemical Society 132 (2010) 7436–7444.